Backbone Dynamics of the N-Terminal Domain in *E. Coli* DnaJ Determined by ^{15}N- and ^{13}CO-Relaxation Measurements†

Kai Huang,‡ Ranajeet Ghose,§ John M. Flanagan,* and James H. Prestegard*

Complex Carbohydrate Research Center, University of Georgia, 220 Riverbend Road, Athens, Georgia 30602-4712, and Department of Biology, Brookhaven National Lab, Upton, New York 11973

Received February 4, 1999; Revised Manuscript Received May 21, 1999

ABSTRACT: The backbone dynamics of the N-terminal domain of the chaperone protein *Escherichia coli* DnaJ have been investigated using steady-state ^{1}H−^{15}N NOEs, ^{15}N T_1, T_2, and $T_{1\rho}$ relaxation times, steady-state ^{13}C$^{\alpha}$−^{13}CO NOEs, and ^{13}CO T_1 relaxation times. Two recombinant constructs of the N-terminal domain of DnaJ have been studied. One, DnaJ(1−78), contains the most conserved "J-domain" of DnaJ, and the other, DnaJ(1−104), includes a glycine/phenylalanine rich region ("G/F" region) in addition to the "J-domain". DnaJ(1−78) is not capable of stimulating ATP hydrolysis by DnaK, despite the fact that all currently identified sites responsible for DnaJ−DnaK interaction are located in this region. DnaJ(1−104), on the other hand, retains nearly the full ATPase stimulatory activity of full length DnaJ. Recently, a structural analysis of these two molecules was presented in an effort to elucidate the origin of their functional differences [Huang, K., Flanagan, J. M., and Prestegard, J. H. (1999) *Protein Science 8*, 203−214]. Herein, an analysis of dynamic properties is presented in a similar effort. A generalized model-free approach with a full treatment of the anisotropic overall rotation of the proteins is used in the analysis of measured relaxation parameters. Our results show that internal motions on pico- to nanosecond time scales in the backbone of DnaJ(1−78) are reduced on the inclusion of the "G/F" region, while conformational exchange on micro- to millisecond time scales increases. We speculate that the enhanced flexibility of residues on the slow time scale upon the inclusion of the "G/F" region could be relevant to the ATPase stimulatory activity of DnaJ if an "induced-fit" mechanism applies to DnaJ−DnaK interactions.

Understanding the molecular mechanism of the biological activities of a protein requires knowledge of both structure and dynamics (*1*). Flexibility of the side-chains and the backbones of residues in regions of contact are often recognized as being necessary for binding substrates and carrying out enzymatic reactions. Residues, which do not directly participate in biological reactions but are involved in the organization of secondary structure elements and the tertiary framework, are more frequently thought of as providing a rigid scaffold on which active sites are presented. However, the case need not be this simple; the backbones of secondary structure segments, and even side-chains buried in the interior of a protein, can possess a certain degree of mobility with characteristic time scales from pico- to milliseconds or longer. These more global internal motions can also be important for a protein in optimizing contacts, particularly when contacts involve the more extended interaction of protein pairs.

Herein, we present a study of the motional properties of the N-terminal domain of *Escherichia coli* DnaJ, which is at the center of some very important regulatory and protein folding processes involving protein−protein interactions. *E. coli* DnaJ is a heatshock protein of about 44 kDa (*2*, *3*). It has been demonstrated in vitro that DnaK, DnaJ, and GrpE act synergistically to refold denatured proteins in an ATP-dependent reaction (*4*). DnaJ plays a key role in regulating the activity of its cochaperone DnaK in the protein refolding reaction. In the presence of ATP, DnaK hydrolyzes ATP and changes its conformation to the ADP-bound form with high affinity for peptide substrates. DnaJ is capable of increasing the rate of the ATP hydrolysis catalyzed by DnaK, thus promoting the ADP-bound state of DnaK and stabilizing the peptide-DnaK complex (*5*, *6*).

The N-terminal domain of DnaJ consists of the highly conserved "J-domain" (residue 1−70) followed by a region abundant in glycine and phenylalanine residues ("G/F" region). Results from biochemical studies have shown that the N-terminal domain of DnaJ is a key player in ATPase stimulatory activity and the binding of DnaJ to DnaK (*7*, *8*, *9*). Several motifs in the "J-domain" have been identified as being critical for the binding (*10*, *11*, *12*, *13*). Nevertheless, the "J-domain" alone does not stimulate ATPase activity of DnaK. A second domain in DnaJ is required for this activity;

† This work was supported by a grant from National Institutes of Health, GM 53181.

* To whom correspondence should be addressed. JMF: Telephone, (516) 344−2792; E-mail, flanagan@bnlbio.bio.bnl.gov. JHP: Telephone, (706) 542-4401; Fax, (706) 542-4412; E-mail, jpresteg@ccrc.uga.edu.

‡ Present address: Laboratory of Chemical Physics, NIDDK, NIH, Bethesda, Maryland 20892.

§ Present address: Universite de Lausanne, Section de Chimie, BCH, CH 1015, Lausanne-Dorigny, Switzerland.

[1] Abbreviations: CPMG, Carr-Purcell-Meiboom-Gill; NOE, Nuclear Overhauser Effects; CSA, Chemical Shift Anisotropy.

10.1021/bi990263+ CCC: $18.00
Published on Web 07/17/1999

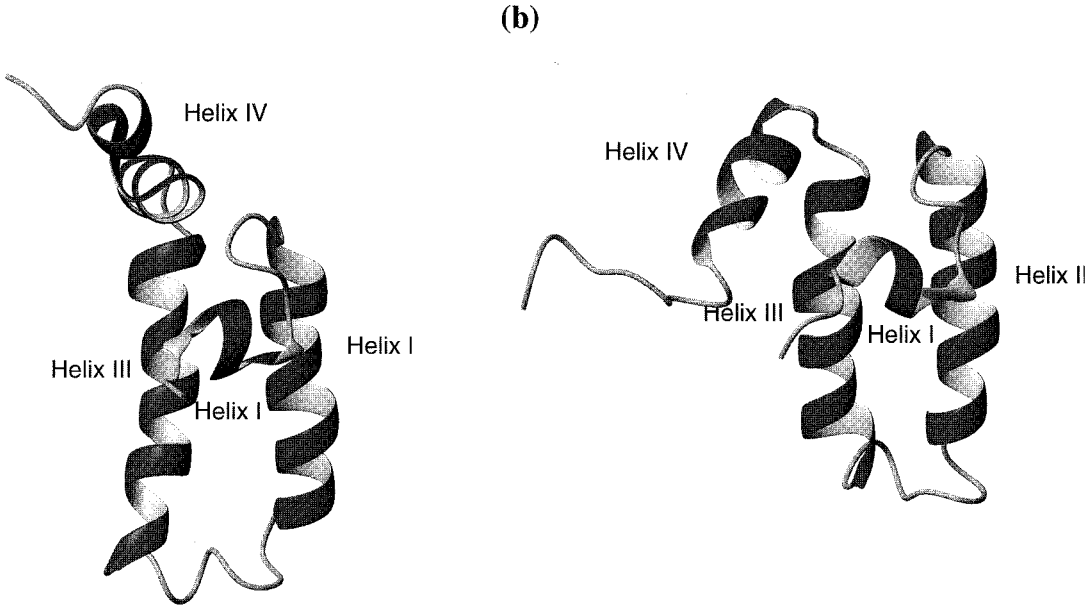

FIGURE 1: Ribbon diagram of the "J-domain" in DnaJ(1−78) (panel a) and DnaJ(1−104) (panel b). The figure was generated with the program MOLMOL (*56*).

it can be either the "G/F" region or an as yet undefined region of the C-terminal domain of DnaJ.

Structural studies have shown that the "J-domain" is highly helical (*14*, *15*, *16*, *17*, *18*). As shown in Figure 1, two central antiparallel helices, helix II and helix III, are connected by a long loop. Two short helices, helix I and helix IV, are found at the N-terminal and C-terminal ends. Helix I and helix IV are connected to helix II and helix III, respectively, by a short turn. The "G/F" region does not appear to have any ordered secondary structure. Nevertheless, an NMR structural comparison of DnaJ(1−78) and DnaJ(1−104) shows that the presence of the "G/F" region induces some structural change in the "J-domain" (*14*). Previously, we have discussed the potential relevance of structural changes in the "J-domain", upon the inclusion of the "G/F" region, to the ATPase stimulatory activity of DnaJ (*14*). Herein, we explore the effect of the "G/F" region on internal motions of the N-terminal domain and discuss the possible functional roles of dynamics.

The relaxation rates of nuclear spin magnetization are a function of molecular motion, thus their measurements can be used to extract information on the internal dynamics of proteins occurring on various time scales. A number of biological processes, including protein folding, ligand binding, and protein recognition, have been probed in this way (*19*, *20*, *21*, *22*, *23*). A model-free approach (*24*, *25*) and an extended model-free approach (*26*) are frequently used to characterize the amplitudes and the time scales of internal motions in a protein that are faster than the overall molecular tumbling rate. These descriptions are based on spin−lattice relaxation times, T_1, spin−spin relaxation times, T_2, and NOE measurements. To study slow conformational changes in the range of micro- to milliseconds, measurements of spin−lattice relaxation times in the rotating frame, $T_{1\rho}$, are quite useful (*27*, *28*, *29*).

^{15}N-relaxation rate measurements have been most widely applied to investigating the correlation between backbone dynamics and mechanisms of biological processes. With the availability of ^{13}C,^{15}N-enriched protein samples, there are increasing interests in using the relaxation rates of ^{13}CO to expand the description of backbone dynamics (*30*, *31*, *32*, *33*). It is possible to probe the anisotropy of motions at various sites along the protein backbone by studying both amide ^{15}N- and ^{13}CO-relaxation (*34*). A few years ago, Pellecchia et al. (*17*) made measurements of ^{15}N-relaxation parameters on a similarly truncated DnaJ, *E. coli* DnaJ(1−107). No efforts were made to extract the amplitudes and the time scales of internal motions of individual N−H bonds using a model-free approach in that study. In this paper, we will describe the results of both ^{15}N- and ^{13}CO-relaxation studies on the N-terminal domain of *E. coli* DnaJ. Because of the nonglobular shape of the two proteins under study, we apply a generalized model-free approach with a full treatment of the anisotropic overall rotation of the proteins. Both ^{15}N-order parameters and ^{13}C$^{\alpha}$-^{13}CO order parameters are calculated to characterize the internal motions of N−H bonds and ^{13}C$^{\alpha}$-^{13}CO bonds, respectively. Moreover, ^{13}C$^{\alpha}$-^{13}CO order parameters are compared to ^{15}N-order parameters of the same residue to detect possible local anisotropic motions. The results show that the inclusion of the "G/F" region has a significant influence on the backbone dynamics of the "J-domain".

EXPERIMENTAL PROCEDURES

Sample Preparation. Uniformly ^{15}N- or ^{15}N,^{13}C-labeled recombinant DnaJ(1−78) and DnaJ(1−104) were expressed in *E. coli* and purified to homogeneity using protocols as described elsewhere (*14*, *16*).

NMR Experiments for Nitrogen-15 Relaxation Measurements. Experiments for ^{15}N-relaxation measurements were executed at 30 °C on a Varian Unity 500 MHz spectrometer equipped with a triple-resonance, pulsed field gradient probe with an actively shielded *z* gradient and a gradient amplifier unit. The ^{15}N spin−lattice (T_1) and spin−spin (T_2) relaxation times and the steady-state ^{1}H−^{15}N NOEs were measured from ^{1}H detected ^{1}H−^{15}N correlation spectra recorded with

sensitivity enhanced pulse sequences. The pulse sequences have been described in detail in the literature (*35*). The reported acquisition parameters were applied in our studies with only minor adjustment. The steady-state $^1H-^{15}N$ NOEs were determined from spectra recorded in the presence and absence of a proton presaturation period of 3 s with a relaxation delay of 5 s. T_2 values were determined from spectra recorded with 5 different durations of the delay T: 16.4, 32.8, 65.6, 98.4, 164.0 ms. Relaxation delays of 1 s between scans were employed. ^{15}N T_1 values were measured from the spectra recorded with seven different durations of the delay T: 54, 118, 200, 299, 426, 617, 935 ms. T_1 spectra were recorded with magnetization relaxing as $exp(-T/T_1)$ and in such a way that the delay between scans affected only the sensitivity and not the extracted T_1 values (*36*). Thus, a short relaxation delay of 1 s was employed between successive scans. All spectra were recorded as 512 × 160 complex matrices with 32 scans per t_1 point. Spectral widths of 1350 and 5500 Hz were employed in frequency domains F_1 and F_2, respectively.

The ^{15}N spin−lattice relaxation rate in the rotating frame, $T_{1\rho}$, was measured using an on-resonance rotating frame experiment. The $T_{1\rho}$ experiment was similar to the one used for the determination of ^{15}N T_2 s, except that the CPMG sequence was replaced by a train of continuous 2 ms low power nitrogen pulses. A spin-lock field strength of 2.4 kHz was employed. Proton refocusing pulses were applied every 4 ms to eliminate the effects of the cross-correlation between $^1H-^{15}N$ dipolar coupling and ^{15}N CSA relaxation mechanisms. $T_{1\rho}$ values were determined from spectra recorded with eight different durations of the delay T: 8, 20, 40, 80, 160, 320, 400 ms. A relaxation delay of 1 s between scans was employed.

NMR Experiments for Carbonyl Carbon-13 Relaxation Measurements. All the ^{13}CO relaxation experiments were carried out at 30 °C on a Varian Unity Plus 600 MHz spectrometer equipped with a triple-resonance, pulsed-field gradient probe with an actively shielded *z* gradient and a gradient amplifier unit. The pulse sequence for T_1 measurement is similar to the one described by Zeng et al. (*33*) except that the magnetization started from H^α protons instead of H^N protons. The H^α proton magnetization was transferred to C^α then to CO with a scheme similar to the CBCA(CO)-HN experiment (*37*). Subsequently, there was a relaxation delay before the magnetization was transferred to the amide nitrogen, then the amide proton for detection. A States-TPPI quadrature detection scheme was used (*38*), and pulsed-field gradients were employed to suppress water and eliminate artifacts in the spectra. A 155 μs G3 (*39*) selective pulse was applied in the middle of the T_1 relaxation delay to suppress the cross correlation between the ^{13}CO CSA and the $^{13}CO-^{13}C^\alpha$ dipolar relaxation mechanisms (*40*, *41*). The T_1 values were determined from eight different relaxation delays T: 5, 100, 200, 400, 600, 800, 1500, 2000 ms. As in the case of ^{15}N measurement, ^{13}CO T_1 spectra were recorded with magnetization relaxing as $exp(-T/T_1)$, and a relaxation delay of 1 s between scans was employed. The pulse sequences for the determination of the steady-state NOE between $^{13}C^\alpha$ and ^{13}CO were the same as the ones described by Zeng et al. (*33*). A relaxation delay of 10.6 s between scans was employed in the NOE measurement experiments.

Data Evaluation. Data processing was performed using Felix (Biosym/Molecular Simulations, San Diego). All spectra were processed with a 90 degree shifted sinebell apodization function applied in both dimensions. The intensities of the peaks in the 2D spectra of ^{15}N-relaxation experiments were taken from peak volumes as measured in Felix. The intensities of the peaks in the 2D spectra of ^{13}CO measurements were taken from peak heights using a Felix macro provided by Professor Arthur Palmer (Columbia University). We have analyzed data using both volumes and peak heights and found no difference in the values of relaxation rates derived. However, in the case of ^{13}CO measurements, because of broader peaks, and less chemical shift dispersion in the CO dimension, the use of peak volumes gave larger deviations in nonlinear data fitting. Thus, we chose to use peak heights in the ^{13}CO relaxation data analysis.

All relaxation rates were determined by fitting the peak intensities to a two-parameter function of the form $I(t) = I_0 exp(-t/T)$, where $I(t)$ is the intensity after a delay of time t and I_0 is the intensity at time $t = 0$. Software developed by Professor Lewis Kay's group was used to extract relaxation rates (*35*).

The offset effects in measurements of the spin−lattice relaxation rate in the rotating frame were taken into account using the following formula (*42*):

$$R_{1\rho}^{eff} = R_1 \cos^2(\beta) + R_{1\rho} \sin^2(\beta)$$

where R_1 is the spin−lattice relaxation rate, $R_{1\rho}$ is the uncorrected spin−lattice relaxation rate in the rotating frame obtained from data fitting, and $\omega_e = (\Delta\omega^2 + \omega_{SL}2)^{1/2}$, where $\Delta\omega$ is the offset between the frequency of the applied spin lock field and the individual amide nitrogen resonance frequency, and ω_{SL} is the spin-lock field strength.

The steady-state $^1H-^{15}N$ NOE values were determined from the ratios of the peak intensities with and without proton saturation. We assumed that the uncertainty in the peak intensities equals the rms background noise in the spectra. The error in the NOEs was estimated using the appropriate error propagation rules from peak uncertainties in the spectra recorded with and without ^1H saturation. The steady-state $^{13}C^\alpha-^{13}CO$ NOE values and the errors in those values were determined in the same manner from spectra recorded with and without $^{13}C^\alpha$ presaturation.

Expressions for the ^{15}N-Relaxation Rates. The T_1 and T_2 relaxation times and the NOE enhancements of an amide ^{15}N nucleus are dominated by the dipolar interaction of the ^{15}N nucleus with its attached proton and by CSA as described by Abragam (*43*):

$$1/T_1 = d^2[J(\omega_H - \omega_N) + 3J(\omega_N) + 6J(\omega_H + \omega_N)] + c^2 J(\omega_N)$$

$$1/T_2 = 0.5d^2[4J(0) + J(\omega_H - \omega_N) + 3J(\omega_N) + 6J(\omega_H) + 6J(\omega_H + \omega_N)] + (1/6)c^2[3J(\omega_N) + 4J(0)]$$

$$NOE + 1 + (\gamma_H/\gamma_N)d^2[6J(\omega_H + \omega_N) - 3J(\omega_N - \omega_N)]T_1$$

The constants d^2 and c^2 are defined as

$$d^2 = \frac{1}{4}\gamma_H^2 \gamma_N^2 \hbar^2 \left\langle \frac{1}{r_{NH}^3} \right\rangle^2$$

$$c^2 = \frac{1}{3}\gamma_N^2 H_0^2 (\sigma_{||} - \sigma_\perp)^2$$

where γ_H and γ_N are the gyromagnetic ratios of the ^{1}H and ^{15}N nuclei, respectively, ω_H and ω_N are the ^{1}H and ^{15}N Larmor frequencies, r_{NH} is the internuclear ^{1}H$-^{15}$N distance (1.02 Å), H_0 is the magnetic field strength, and the parallel and perpendicular components of the assumed axially symmetrical ^{15}N-chemical shift tensor are represented by $\sigma_{||}$ and $\sigma_\perp$, respectively. A $\sigma_{||} - \sigma_\perp$ value of -160 ppm was used for the amide nitrogen chemical shifts considered here (*44*). $J(\omega)$ is a spectral density function, which describes the frequency distribution of motions that modulates chemical shift anisotropies and dipolar interactions.

Additional motional dependence of T_2 can arise from chemical exchange processes, such as slow conformational interconversions, that are normally not considered a part of the $J(\omega)$ described above. When this happens, $T_{1\rho}$ becomes an important variable for separating exchange contributions. An expression for $T_{1\rho}$ in terms of additional spectral density function contributions and effective magnetic field parameters was developed by Peng et al. (*45*) using a semiclassical formalism. In the limit of a weak on-resonance spin lock field, and an assumption of a Lorentzian spectral density function equal to that introduced above in the absence of exchange, $T_{1\rho}$ provides the same spectral information as T_2. Hence, the $T_{1\rho}/T_2$ ratio is expected to be one when the above conditions are satisfied. When an exchange process is present, the $T_{1\rho}/T_2$ ratio, however, may significantly deviate from one. Therefore, the $T_{1\rho}/T_2$ value can be used to screen for the presence of an exchange process in proteins.

The contribution of exchange processes to T_2 and $T_{1\rho}$ can be analyzed by explicitly including an exchange contribution to relaxation rates, R_{ex}, as follows:

$$1/T_2 = 1/T_2^\infty + R_{ex},\ 1/T_{1\rho} = 1/T_{1\rho}^\infty + R_{ex}^{1\rho}$$

Here, T_2^∞ is the spin$-$spin relaxation time in the absence of exchange, and $T_{1\rho}^\infty$ is the spin$-$lattice relaxation time in the rotating frame in the absence of exchange. T_2^∞ and $T_{1\rho}^\infty$ should have approximately the same value.

In the fast-exchange regime, the contribution from the exchange process to T_2 is

$$R_{ex} = p_A p_B \Delta\Omega^2 \tau_{ex}$$

in which p_A and p_B are the populations of different conformational or chemical states A and B. $\Delta\Omega$ is the chemical shift difference between state A and state B, and τ_{ex} is the time constant for the exchange process. The exchange term contributes to $T_{1\rho}$ in a similar way, but it is modified by the strength of the spin-lock RF field ω_{SL} (*27*)

$$R_{ex}^{1\rho} = p_A p_B \Delta\Omega^2 \frac{\tau_{ex}}{1 + \omega_{SL}^2 \tau_{ex}^2}$$

The magnitude of the spin lock field usually is a few kHz. Therefore, for an exchange process with a τ_{ex} on the order of a milli-second, the $1 + \omega_{SL}2\tau_{ex}2$ factor in $R_{ex}^{1\rho}$ is large, and $T_{1\rho}$ relaxation times are affected much less by exchange. Under these circumstances, a $T_{1\rho}/T_2$ ratio larger than 1.0 will be observed.

Model-Free Interpretation of ^{15}N-Spectral Density Functions. The model-free approach has been widely used to extract dynamical information from nuclear magnetic relaxation data. In its simplest form, the internal dynamics of a nuclear spin is described by only two parameters: a motional correlation time, τ_e, and an order parameter, S, that describes spatial restriction of the motion (*24*, *25*). The overall motion of the protein in the isotropic tumbling limit is characterized by an overall correlation time, τ_m. The corresponding spectral density function is then

$$J(\omega) = \frac{S^2\tau_m}{1 + \omega^2\tau_m^2} + \frac{(1 - S^2)\tau}{1 + \omega^2\tau^2}$$

with $1/\tau = 1/\tau_m + 1/\tau_e$.

In the case where the time evolution of the internal reorientational motion contains a significant component at a slow time scale, it may not be sufficient to use a single τ_e. An extended form of the model free approach was developed by Clore et al. (*26*) to analyze relaxation rates in such situations. Assuming that internal motions take place on two distinct time scales differing by at least an order of magnitude, and that the term containing the correlation time describing the faster of the two time scales contributes a negligible amount to the relaxation, the modified spectral density function becomes

$$J(w) = \frac{S^2\tau_m}{(1 + \omega^2\tau_m^2)} + \frac{(S_f^2 - S^2)\tau}{(1 + \omega^2\tau^2)}$$

where the square of the order parameter S^2 is expressed as the square of the product of two order parameters characterizing the fast and slow internal motion, S_f^2 and S_s^2, respectively. The effective correlation time for the slow internal motions, τ_s, is included using the relationship $1/\tau = 1/\tau_s + 1/\tau_m$.

In the case of anisotropic overall rotation, it is not sufficient to describe the overall tumbling using a single correlation time τ_m. In the most general case, five correlation times are needed (*46*). The correlation times are given in terms of elements of a rotational diffusion tensor as follows:

$$\tau_1 = (4D_{xx} + D_{yy} + D_{zz})^{-1},\ \tau_2 = (D_{xx} + 4D_{yy} + D_{zz})^{-1}$$

$$\tau_3 = (D_{xx} + D_{yy} + 4D_{zz})^{-1},\ \tau_4 = [6D + 6(D^2 - L^2)^{1/2}]^{-1}$$

$$\tau_5 = [6D - 6(D^2 - L^2)^{1/2}]^{-1}$$

where $D = (D_{xx} + D_{yy} + D_{zz})/3$, and $L^2 = (D_{xx}D_{yy} + D_{xx}D_{zz} + D_{yy}D_{zz})/3$. The spectral density function is the Fourier transformation of the autocorrelation function,

$$J(\omega) = S^2 \sum_{k=1-5} \frac{a_k\tau_k}{1 + \omega^2\tau_k^2} + \frac{(1 - S^2)\tau}{1 + \omega^2\tau^2}$$

where $1/\tau = 1/\tau_{iso} + 1/\tau_e$. τ_{iso} is the effective isotropic rotational correlation time. For large molecules in the absence of exchange, τ_{iso} can be measured by relating it to a ratio of T_1 to T_2. The coefficients a_k are given by

$$a_1 = 6m^2n^2,\ a_2 = 6l^2n^2,\ a_3 = 6l^2m^2,\ a_4 = d - e,\ a_5 = d + e$$

where m, n, l are the direction cosines of the N−H vector with respect to the diffusion axes x, y, and z, respectively, and d and e are given by the following expressions:

$$d = [3(l^4 + m^4 + n^4) - 1]/2$$

$$e = [\delta_x(3l^4 + 6m^2n^2 - 1) + \delta_y(3m^4 + 6l^2n^2 - 1) + \delta_z(3n^4 + 6l^2m^2 - 1)]/6$$

$$\delta_i = (D_{ii} - D)/(D^2 - L^2)^{1/2}$$

The software package DASHA (*47*), which contains the subroutines for the analysis of N−H relaxation data using a model-free approach in the case of anisotropic overall rotation, was used in our study. To determine the overall rotational correlation times, we must know the direction cosines of the N−H vectors with respect to the diffusion tensor axes and the molecular diffusion constants. Both can be estimated from existing three-dimensional structures of the protein. The beads model, in which the shape of the protein is defined by a large number of spherical subunits, was used to represent the hydrodynamic properties of the protein (*48*, *49*, *50*).

We selected all the α carbon atoms from the pdb files of our NMR structures of the N-terminal domain of DnaJ (*34*) as the "beads". The effective hydrodynamic radius of a bead was assumed to be proportional to the square root of the accessible surface area of the bead, thus allowing for a reduction in the hydrodynamic radius from its initial van der Waals radius of 1.75 Å due to overlap with its neighbors (*51*). The accessible surface area was calculated using the Lee & Richards (*52*) algorithm with a probe size of 1.6 Å and a scaling factor of 1.0. If the radius of the friction point became smaller than 0.1 Å after a scaling factor was included, the friction point was discarded. Note that for DnaJ-(1−104), because the structure of the "G/F" domain is in disorder and not defined, only the "J-domain" was taken into account in the hydrodynamics calculation.

The experimental relaxation data were ultimately fit to five different models: (1) internal motion characterized by S^2 with τ_e fixed to zero; (2) internal motion characterized by S^2 and τ_e; (3) internal motion characterized by S^2 with τ_e fixed to zero, and an exchange process characterized by R_{ex}; (4) internal motion characterized by S^2, τ_e, and an exchange process characterized by R_{ex}; (5) internal motions characterized by S_s^2, τ_s, and S_f^2. The parameters characterizing internal motions were extracted from the experimental relaxation data by minimization of the loss function, χ^2, using the Newton−Raphson minimization algorithm,

$$\chi^2 = \frac{(T_{1c} - T_{1e})^2}{\sigma_{T1}^2} + \frac{(T_{2c} - T_{2e})^2}{\sigma_{T2}^2} + \frac{(NOE_c - NOE_e)^2}{\sigma_{NOE}^2}$$

where the variables with an index c are theoretical values and the variables with an index e are experimental values.

The criteria for selecting the appropriate model from which to calculate a spectral density function for each residue were the following: (1) χ^2 must be less than a critical value corresponding to a 95% confidential limit; (2) the error in the extracted value of model-free parameters must not be larger than the value of the parameters; (3) if there were several models satisfying criterion 1 and 2, an F-test (*53*) was applied (vide infra) to decide if the model with a lower number of degrees of freedom was statistically better than the model with a larger number of degrees of freedom. If the two models had the same number of degrees of freedom, we would choose the model with smaller χ^2 value; (4) since model 5 has zero degrees of freedom, it was selected only when there was no other model satisfying the model selection criteria 1 and 2. In the F-test, the F value was calculated as

$$F = \frac{p_2(\chi_1^2 - \chi_2^2)}{(p_1 - p_2)\chi_2^2}$$

in which p_1 and p_2 ($p_1 > p_2$) are the number of degrees of freedom. The model with less freedom was considered statistically better than the model with more freedom, if the F value was larger than 0.1.

Model-Free Analysis of ^{13}CO Relaxation Rates. There are some complications in extracting carbonyl carbon order parameters from relaxation rates. For instance, unlike the ^{15}N-chemical shielding, the assumption of an axially symmetrical shift tensor for ^{13}CO is not valid, and principle components are not conveniently oriented along bonds. Hence, it is necessary to know all components of the chemical shift tensor in order to construct the expression for T_1, T_2, and NOEs from spectral density functions. While approximate values are known, these values are more sensitive to both amino acid type and structural environment than ^{15}N-chemical shift tensor components (*32*).

Nevertheless, sensitivity to these details can be minimized and an approximate description of the local motion of the C^α−CO bond can be derived from an analysis of the ^{13}CO T_1 and the C^α−CO steady-state NOEs. The steady-state NOE can be written as

$$NOE = I_{sat}/I_0 = 1 + \sigma T_1$$

from which σ, the dipolar cross relaxation rate between $^{13}C^\alpha$ and ^{13}CO, can be determined. In analogy to our previous equation for a ^{1}H−^{15}N NOE, the $^{13}C^\alpha$−^{13}CO cross relaxation rate can be expressed in terms of a spectral density function as

$$\sigma = d^2[6J(\omega_{C\alpha} + \omega_{CO}) - J(\omega_{C\alpha} - \omega_{CO})]$$

with

$$d = \frac{1}{2}\gamma_c^2\hbar\left\langle\frac{1}{r_{C\alpha CO}^3}\right\rangle$$

Since ω_{C^α} and ω_{CO} are very similar, the above expression can be simplified to

$$\sigma = d^2[6J(2\omega_C) - J(0)]$$

In proteins at high fields, $J(0) \gg J(2\omega_C)$, and thus the latter term can be neglected. In the model-free approach,

$$J(0) = S^2 \sum_{i=1-5} a_i\tau_i + (1 - S^2)\tau$$

where the spectral density coefficients, a_i, can be derived from the direction cosines of the $C^{\alpha}-CO$ bond with respect to the diffusion axes. Note that the values of these coefficients are different from those for N−H bonds since the direction cosines are different. The second term in the above expression can usually be neglected because τ is much shorter than τ_i. In this limit, we get a simple expression for the $^{13}C^{\alpha}-^{13}CO$ order parameter,

$$S^2 = \frac{-\sigma}{d^2 \sum_{i=1-5} a_i\tau_i}$$

RESULTS

Measured Nitrogen-15 Relaxation Parameters. The average T_1, T_2, $T_{1\rho}$, and NOEs for DnaJ(1−78) are 481 ± 49, 150 ± 36, 134 ± 14, and 0.65 ± 0.14 ms, respectively. The corresponding average values for residues in the "J-domain" in DnaJ(1−104) are 562 ± 51, 97 ± 19, 116 ± 16, and 0.73 ± 0.16 ms, respectively. The N-terminal residues in both proteins, such as Gln 3, and residues in the "G/F" region in DnaJ(1−104) consistently have longer values of T_1 and T_2, and lower values of the steady-state $^1H-^{15}N$ NOEs. This is indicative of flexibility in the backbone on the picosecond to 100 picosecond time scale. These results agree with the previous structural characterization and amide proton exchange rates for the DnaJ(1−104) construct, which showed both the N-terminus and the "G/F" region to be in structural disorder (*14*). The results also compare well to observations made on a DnaJ(1−107) construct (*17*). We also observe longer values of T_1 and T_2, and lower values of steady-state $^1H-^{15}N$ NOEs for residues Glu 74 and Gln 75 in DnaJ(1−78) than we do in DnaJ(1−104). These residues are near the C-terminus in DnaJ(1−78), and some deviation upon removal of the "G/F" region would be expected. Deviations from the average values of relaxation rates are observed in other regions as well, such as the loop connecting helix II and helix III. However, those deviations are more complicated and cannot be directly interpreted without further analysis using the model-free approach.

The values of the $T_{1\rho}/T_2$ ratios as a function of residue number for DnaJ(1−78) and DnaJ(1−104) are shown in Figure 2. The average $T_{1\rho}/T_2$ ratio is 0.93 ± 0.06 for DnaJ(1−78). The deviation from one is nearly within our calculated standard deviation from the mean and is also within our estimated experimental precision. Thus, we do not consider the value of the $T_{1\rho}/T_2$ ratio to indicate significant levels of slow internal motion. The average $T_{1\rho}/T_2$ ratio for the residues in the "J-domain" DnaJ(1−104) is 1.23 ± 0.20. While the deviation from one again appears to be near the calculated deviation from the mean, the scatter is more than 3× as large as that in DnaJ(1−78), and for a number of residues, the deviations are clearly more than the experimental precision might have allowed. Such residues include Val 11, Ser 12, Tyr 31, Asp 34, Ala 44, Phe 46, Tyr 68, Ala 71, and Glu 74. The observation suggests that for DnaJ(1−104) there could be exchange processes in the 100 μs − 1 ms range occurring in the regions where those residues are located.

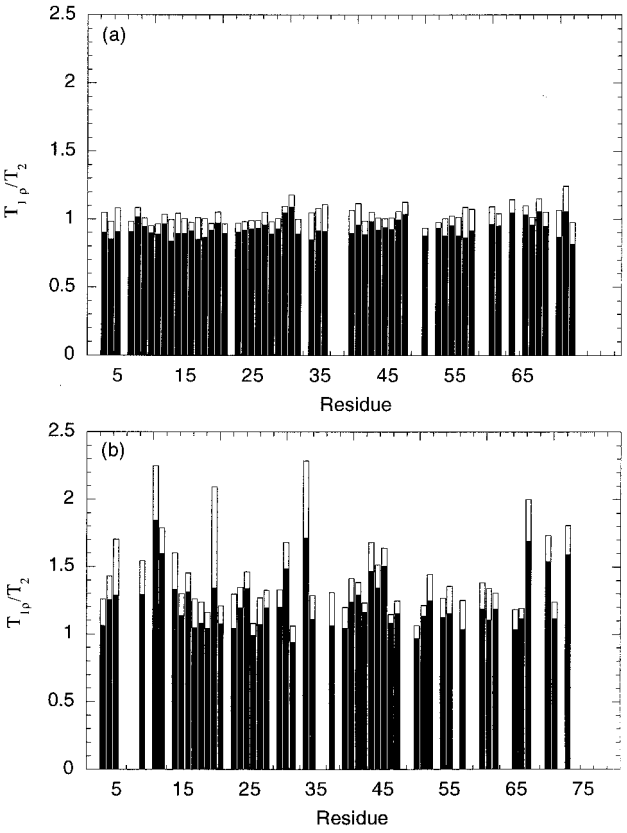

FIGURE 2: A plot of $T_{1\rho}/T_2$ ratio as a function of residue number for DnaJ(1−78) (panel a) and DnaJ(1−104) (panel b).

The T_1/T_2 ratio is closely related to an effective isotropic τ_m, with a higher ratio reflecting slower tumbling (*35*). The rotational correlation time τ_m estimated from the values of ^{15}N T_1/T_2 is 5.6 ns for DnaJ(1−78). Those values of the T_1/T_2 ratio that deviate from the average by more than one standard deviation are not used in this calculation, assuming that other factors such as chemical exchange might contribute to these values. Because of the significant exchange contribution to the ^{15}N T_2 values in DnaJ(1−104), $T_{1\rho}$ instead of T_2 values are used in the τ_m estimation for DnaJ(1−104). Moreover, the $T_1/T_{1\rho}$ ratios of the residues in the "G/F" region are excluded in the calculation. The estimated τ_m is 7.4 ns for DnaJ(1−104). The relative size of the τ_m values approximately scales with the molecular weight of these two proteins.

Estimation of Effective Isotropic Rotational Correlation Time. The ratios of eigenvalues of the rotation diffusion tensor calculated using the anisotropic structure model of our proteins are 1.0:1.0:0.3 and 1.0:0.9:0.5 for DnaJ(1−78) and DnaJ(1−104), respectively. The effective isotropic rotational correlation time can also be calculated directly from the hydrodynamics calculation. The values obtained are 2.9 ns for DnaJ(1−78) and 3.1 ns for DnaJ(1−104), excluding the "G/F" region. These values are low compared to values derived from NMR experiments. It is, however, well-known that including a solvent shell increases the values of correlation times (*54*, *55*). Because of the difficulties in estimating the thickness of the hydration layer and because of the additional complication of treating the "G/F" region in DnaJ(1−104), we decided to use a semiempirical approach

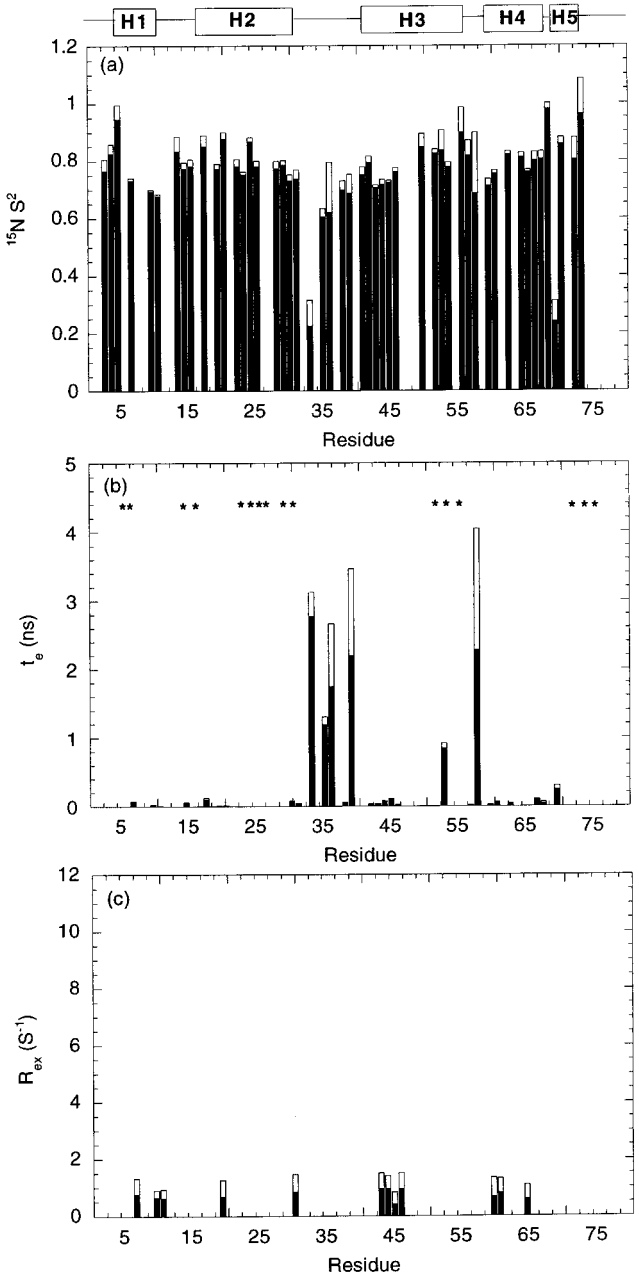

FIGURE 3: Values of model-free parameters plotted versus the amino acid sequence for DnaJ(1−78). Residues requiring a two-time scale model are labeled by * in panel (b). The secondary elements are indicated with boxes.

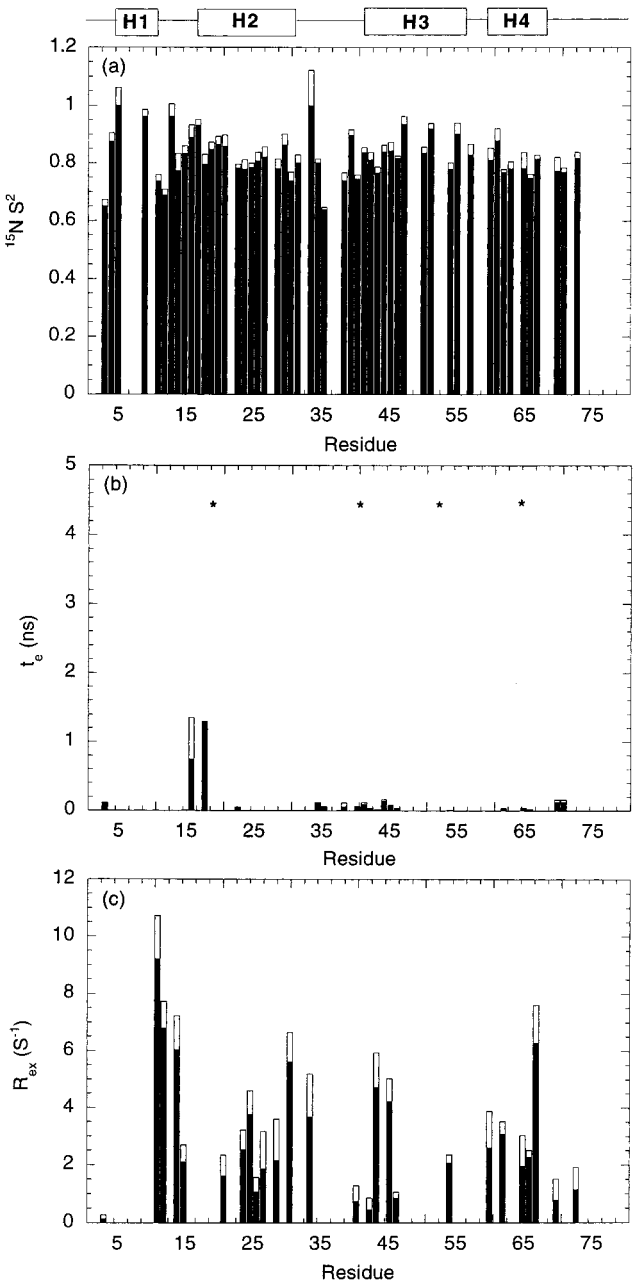

FIGURE 4: Values of model-free parameters plotted versus the amino acid sequence for DnaJ(1−104). Residues requiring a two-time scale model are labeled by * in panel (b). The secondary elements are indicated with boxes.

to converting diffusion times to anisotropic correlation times. We basically assume that anisotropy is appropriately represented, and scale each τ_i by a factor, τ_m/τ_{iso}. Here, τ_{iso} is the overall effective isotropic rotational correlation time given by the hydrodynamic calculation without a solvent shell and τ_m is the overall effective isotropic rotational correlation time determined from a T_1/T_2 ratio. The rotational correlation times scaled by τ_m/τ_{iso} are $\tau_1 = 7.1$, $\tau_2 = 7.1$, $\tau_3 = 3.9$, $\tau_4 = 3.9$, $\tau_5 = 9.7$ ns for DnaJ(1−78), and $\tau_1 = 8.6$, $\tau_2 = 8.2$, $\tau_3 = 6.0$, $\tau_4 = 6.0$, $\tau_5 = 10.0$ ns for DnaJ(1−104).

Model-Free Analysis. Values of model-free parameters and R_{ex} terms for each residue can be derived from nitrogen relaxation rates using the calculated anisotropic diffusion parameters of DnaJ(1−78) and DnaJ(1−104). The results are shown in Figure 3 and Figure 4. When a 2 time scale model is used, only S^2_f values are shown. These values are equivalent to the S^2 values characterizing single time scale internal motions since both are indications of the amplitude of internal motions on sub-nanosecond time scales.

The models required to fit the relaxation data of the residues in the "J-domain" are quite different for DnaJ(1−78) and DnaJ(1−104). In DnaJ(1−78), 16 residues require a 2 time scale model that includes a second slower internal motion to fit the experimental data. A few of those residues are in the N-terminal and C-terminal region, while most of them are in helix II. Even when a single time scale model is used to fit the data, many τ_e are quite long. This is particularly true in the loop region between helix II and helix III. There are just 12 residues in DnaJ(1−78) requiring an exchange term, and the R_{ex} terms in DnaJ(1−78) are less than 1 s^{-1}. In DnaJ(1−104), there are only four residues

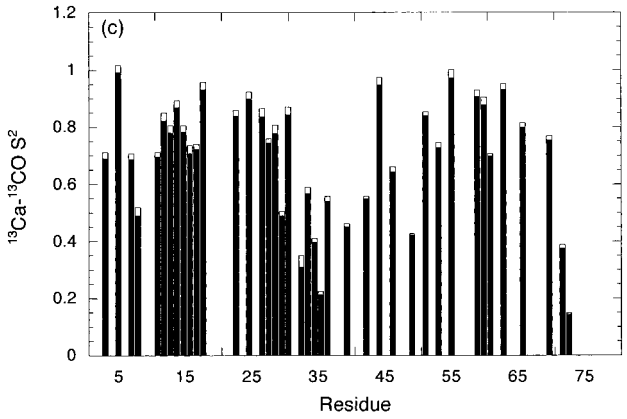

FIGURE 5: Values of $^{13}C_\alpha-^{13}CO$ order parameters plotted versus the amino acid sequence for DnaJ(1−78).

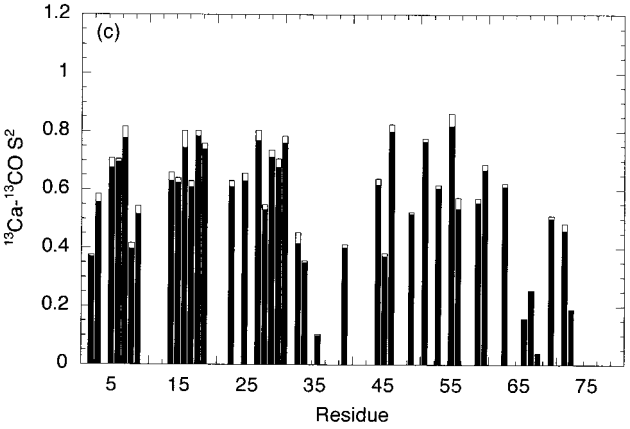

FIGURE 6: Values of $^{13}C_\alpha-^{13}CO$ order parameters plotted versus the amino acid sequence for DnaJ(1−104).

requiring a 2 time scale model and only one of them is in helix II. Also, the τ_e values from the single parameter fits tend to be smaller. However, there are as many as 26 residues in DnaJ(1−104) requiring an exchange term, and 21 of them have an R_{ex} term larger than 1 s^{-1}. Thus, there appears to be a shift from internal motion on the 10−100 ps time scale to more extended motion on the 1 μs − 1 ms time scale when the "G/F" region is added.

The relaxation data for the residues in the "G/F" region itself were analyzed using an isotropic model since it was not possible to obtain anisotropic parameters for them. A rotational correlation of 3.7 ns, which was estimated by T_1/T_2 ratios of the residues in this region, was used in the model-free analysis. Only residues Met 78, Ala 87, Asp 88, Ser 90, and Asp 91 produced acceptable fits with one of the five models. All resulting fits showed an order parameter near zero.

Studies of Carbonyl Carbon-13 Relaxation. The values of the ^{13}CO T_1, $^{13}C^\alpha-^{13}CO$ NOEs, and $^{13}C^\alpha-^{13}CO$ order parameters of residues in DnaJ(1−78) and DnaJ(1−104) are plotted in Figure 5 and Figure 6. Because of chemical shift degeneracy, few residues in the "G/F" region could be analyzed reliably. Thus, we only show residues in the "J-domain" for DnaJ(1−104) in Figure 6. The average values of T_1, NOEs, and S^2 for DnaJ(1−78) are 1.53 ± 0.08, 0.874 ± 0.039, and 0.694 ± 0.214 s. The corresponding average values for DnaJ(1−104) are 1.48 ± 0.14, 0.880 ± 0.037, and 0.555 ± 0.200 s. There is no significant variation in the values of carbonyl T_1 values throughout the "J-domain", except for Lys 61, Ala 64 in DnaJ(1−78), and Thr 57 in DnaJ(1−104). $^{13}C^\alpha-^{13}CO$ NOE values are quite uniform as well with only a few residues deviating significantly from the average. In DnaJ(1−78), those residues are Lys 30, Pro 33, Arg 35, Asn 36, Phe 73, and Glu 74. In DnaJ(1−104), those residues are Asn 36, Gln 67, Tyr 68, Gly 69, and Glu 74. The values for the $^{13}C^\alpha-^{13}CO$ order parameters are not as uniform as T_1 and NOE values, partly because of increased errors. In general, residues in the loop region and the C-terminal region following helix IV have significantly lower order parameters. Complete tables of relaxation data and derived parameters for both ^{13}CO and ^{15}N are included in the Supporting Materials.

DISCUSSION

The average values of ^{15}N order parameters for helix I−helix IV in DnaJ(1−78) are 0.799 ± 0.112, 0.796 ± 0.047, 0.774 ± 0.051, 0.776 ± 0.041 s. As expected, these values, which reflect increasing amplitude of internal N−H vector motion as they decrease from an upper limit of one, are quite close to one and are quite similar to each other in these helical regions. In an α helix, N−H vectors are all hydrogen bonded to the carbonyl groups in the amino acid four residues away; the local environment is quite similar, quite restricted, and at least at fast time scales, the spatial freedom of these N−H vectors should not differ greatly. In helix III, however, residues in the first half of the helix seem to have an lower value of order parameter than those residues in the second half of the helix. The average value of order parameters for residues 42−47 is 0.74 ± 0.03, and the value for residues 51 to 55 is 0.82 ± 0.03. Both Pellecchia et al. (*17*) for the DnaJ(1−107) construct and we for the DnaJ(1−78) and DnaJ(1−104) constructs (*14*), have shown previously that the amide proton exchange rates in the first half of helix III are in the intermediate range so that they cannot be observed in either a D_2O exchange experiment or in a magnetization transfer experiment. Thus, the difference in order parameters observed herein seems to correlate with the difference observed in amide proton exchange rates. There are a few residues, such as Gly 10 and Val 11 in the turn between helix I and helix II, and Asp 34 and Asn 36 in the loop connecting helix II and helix III, that have order parameters significantly lower than the average. These residues apparently experience more flexibility than those residues in helices.

There is a significant amount of motion on time scales of pico- to nanoseconds in the backbone dynamics of DnaJ-(1−78), as indicated by the requirement of a 2 time scale model or a large τ_e value for many residues in order to produce an adequate fit to the ^{15}N-relaxation data. On the other hand, there seems to be few slow time scale exchange processes in DnaJ(1−78), suggested by the observation that the exchange terms required to fit the relaxation data are small (less than 1), and that the $T_{1\rho}/T_2$ ratios are not significantly deviated from one.

The values of the $^{13}C^\alpha-^{13}CO$ order parameter indicate that the N-terminal region, C-terminal region, and the loop region are more flexible than the rest of the molecule. This is consistent with the results from the ^{15}N-relaxation studies. Moreover, as shown in Figure 7, most residues show a fairly good agreement between the magnitude of the ^{15}N and $^{13}C^\alpha-$

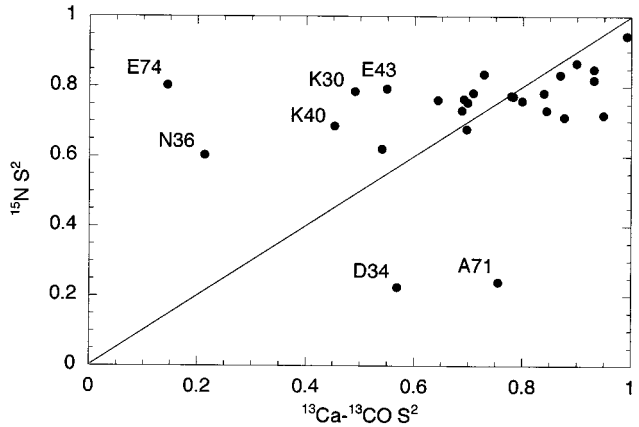

FIGURE 7: Values of $^{13}C_\alpha-^{13}CO$ order parameters plotted versus ^{15}N order parameters for residues in the "J-domain" in DnaJ(1−78). Residues showing poor correlation between $^{13}C_\alpha-^{13}CO$ order parameters and ^{15}N order parameters are labeled.

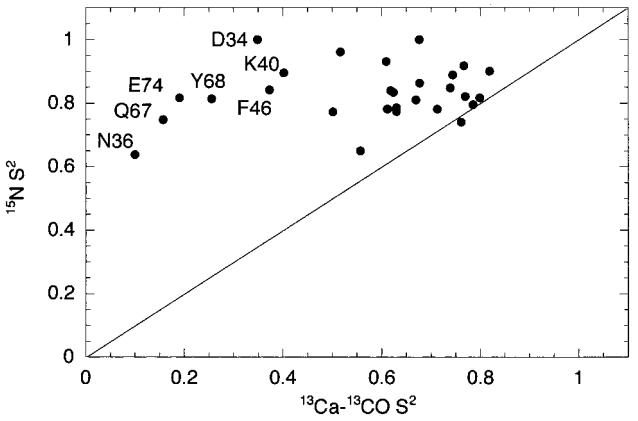

FIGURE 8: Values of $^{13}C_\alpha-^{13}CO$ order parameters plotted versus ^{15}N order parameters for residues in the "J-domain" in DnaJ(1−104). Residues showing poor correlation between $^{13}C_\alpha-^{13}CO$ order parameters and ^{15}N order parameters are labeled.

^{13}CO order parameters. Since the ^{15}N-order parameters reflect mainly the internal motion of the N−H bonds, and $^{13}C^\alpha-^{13}CO$ order parameters reflect the internal motion of the $C^\alpha-CO$ bonds, the consistency between the ^{15}N and ^{13}CO order parameters is not unexpected when these two bonds are part of a rigid peptide plane undergoing near symmetric internal reorientation. A few residues, such as Asp 34 and Asn 36 in the loop region, and Ala 71 and Glu 74 in the C-terminus, do not have a good correlation between the $^{13}C^\alpha-^{13}CO$ order parameters and ^{15}N order parameters. They are all in flexible regions, and their internal motions along directions sampled by the various ^{15}N- and ^{13}C-interactions are more likely to be anisotropic.

Changes in the backbone dynamics of the "J-domain" are observed when the "G/F" region is included. In DnaJ(1−104), the average value of ^{15}N order parameters for each helix are 0.945 ± 0.065, 0.825 ± 0.056, 0.812 ± 0.125, 0.836 ± 0.059. Compared to corresponding segments in DnaJ(1−78), there is a small but significant increase throughout the molecule. Moreover, residue Asp 34 has a very high order parameter in DnaJ(1−104). In concert with the slight increase in ^{15}N order parameters for DnaJ(1−104) over DnaJ(1−78), we find less need to fit relaxation data with models that include internal motions on the time scale of picoseconds to nanoseconds. It seems that by including the "G/F" region, the very rapid backbone internal motions of the "J-domain" are significantly damped. Despite the reduction in the amount of fast motion in DnaJ(1−104), a large number of residues seem to be involved in slower exchange processes on the time scale of micro- to milliseconds. Very large R_{ex} terms are found in residues Val 11, Ser 12, Thr 14, Lys 25, Tyr 31, Asp 34, Ala 44, Phe 46, and Tyr 68.

As shown in Figure 8, the overall $^{13}C^\alpha-^{13}CO$ order parameters seem to be lower than the values of the ^{15}N order parameter for DnaJ(1−104). It has been suggested that the concerted helix movement about the C═O bond direction will cause a lower value of $^{13}C^\alpha-^{13}CO$ order parameters than that of the ^{15}N order parameter (*34*). It is possible that the addition of the "G/F" region results not only in damping of the amplitude of rapid local motions, but an increase in amplitude of slower more anisotropic motion for helical segments. In addition, individual residues such as Leu 9, Asp 34, Asn 36, Lys 40, Phe 46, Gln 67, Tyr 68, and Glu 74 show much less correlation between $C^\alpha-CO$ order parameters and ^{15}N order parameters in DnaJ(1−104). These residues may have different kinds of anisotropic motion from other parts of the molecule.

ATP hydrolysis is the rate-limiting step in the DnaK/DnaJ ATPase cycle that locks protein/peptide substrates into the substrate binding cavity of DnaK. This key step is strongly stimulated by the DnaJ cochaperone. To associate the characteristics of the backbone dynamics of the "J-domain" with its functions and understand the mechanism by which the "G/F" region may modulate the interaction between DnaJ and DnaK, we will focus further discussion on the sites that are suggested to be responsible for the DnaJ−DnaK interaction and the ATPase stimulatory activity. Results from NMR titration experiments with DnaJ(1−74) and DnaK indicate that the DnaK binding sites are localized in the outer face of helix II, residues Val 11 and Ser 12 in the turn region near the N-terminus of helix II, and the "HPD" tripeptide following the C-terminus of helix II (*13*). The 32H−33P−34D tripeptide segment in the loop region is required for the ATPase activity of DnaJ and binds along a channel in the ATPase domain of DnaK (*57*, *58*). A second binding determinant in DnaK is likely to be in the substrate binding domain because mutations in the vicinity of the substrate binding pocket have either a reduced rate and or affinity for DnaJ binding (*58*). The current model suggests that DnaJ binding may propagate conformational changes between the ATPase and substrate-binding domains. The changes in dynamical behavior of helix II on adding the "G/F" region are in general not dissimilar from those of other helices, but Lys 25 and Tyr 31, which are on the outer edge of the helix, do change significantly. Also, the changes in the loop and turn regions do stand out. Asp 34, for example, is very flexible in DnaJ(1−78), but adopts a very high ^{15}N order parameter, a big R_{ex} term, and a low $^{13}C^\alpha-^{13}CO$ order parameter in DnaJ(1−104). Residues in the turn region also exhibit an elevated level of slow conformational exchange on addition of the "G/F" region. Consistent with this latter observation, we have reported previously that amide proton exchange rate constants of residues 10−15 change significantly in the presence of the "G/F" region (*14*).

Another site that has been suggested to be responsible for DnaJ−DnaK interaction is the QKRAA amino acid motif

(residue 60−64) in helix IV (*11*). In the NMR titration studies with DnaJ(1−74), this region is not found to be sensitive to the presence of DnaK. So, it is possible that the conformation of helix IV in DnaJ(1−74) simply makes it less accessible to DnaK. More importantly, our structural studies have shown that the packing of helix IV is different in the presence of the "G/F" domain (*14*), and in the current study, we see modest changes in the size of Rex terms in this region.

The apparent increase in slow motions of particular sites along the "J-domain" backbone on adding the "G/F" region may be associated with the molecular mechanism of DnaJ−DnaK interaction in several ways. If they are large in amplitude, then slow motions could be important in promoting the protein−protein interaction via an "induced-fit" mechanism. Recent mechanistic studies of ATPase stimulation by DnaJ have emphasized the complexities of the DnaJ/DnaK/peptide interactions that are necessary for ATPase stimulation (*59*) and the likelihood that the mechanism involves induced conformation changes in the proteins (*60*). On the basis of the short T_2 value of Asp 34 and the critical role of the "32H-33P-34D" tripeptide in DnaJ−DnaK interaction, Pellecchia et al. (*17*) have previously speculated that the loop containing the tripeptide is a good candidate for an "induced-fit" mechanism in the interactions with DnaK. Our data support the existence of slow motions in the tripeptide region as well as the V11−S12 turn region and K25, Y31 side of helix II. Therefore, it is not unreasonable to suggest that the flexibility of residues on the entire protein−protein interaction interface may be necessary for an appropriate DnaJ−DnaK interaction. The dynamic properties of the "G/F" region may also play a role in facilitating entry of residues in the J-domain into the channel in DnaK and aid in transmitting information between the ATPase and substrate-binding domains of DnaK.

ACKNOWLEDGMENT

The pulse sequences for the measurements of ^{15}N T_1, T_2, and steady-state $^1H-^{15}N$ NOE were kindly provided by Professor Lewis Kay (University of Toronto). The Felix macro for extracting peak height was kindly provided by Professor Arthur Palmer (Columbia University). KH also thanks Dr. Neil Farrow (Du Pont) for providing his software for ^{15}N-relaxation data analysis, and Jon Lapham (Yale University) for his help in calculating inertia tensors.

SUPPORTING INFORMATION AVAILABLE

The following information is available as supporting materials: (1) summaries of the ^{15}N-relaxation parameters of DnaJ(1−78) and DnaJ(1−104), including values of T_1, T_2, $T_{1\rho}$, and $^1H-^{15}N$ NOE; (2) summaries of ^{13}CO relaxation parameters of DnaJ(1−78) and DnaJ(1−104), including values of $^{13}C^{\alpha}-^{13}CO$ NOE, $^{13}C^{\alpha}-^{13}CO$ dipolar cross-relaxation rate, and $^{13}C^{\alpha}-^{13}CO$ order parameters; (3) model-free parameters and average order parameter values for each secondary structure element in DnaJ(1−78) and DnaJ(1−104); (4) the pulse sequence for ^{13}CO T_1 measurement. This material is available free of charge via the Internet at http://pubs. acs. org.

REFERENCES

1. Jardetzky, O. (1996) *Prog. Biophys. Mol. Biol. 65*, 171−219.
2. Bardwell, J. C. A., Tilly, K., Craig, E., King, J., Zylicz, M., and Georgopoulos, C. (1986) *J. Biol. Chem. 261*, 1782−1785.
3. Ohki, M., Tamura, F., Nishimura, S., and Uchida, H. (1986) *J. Biol. Chem. 261*, 1778−1781.
4. Langer, T., Lu, C., Echols, H., Flanagan, J., Hayer, M. K., and Hartl, F. U. (1992) *Nature 356*, 683−689.
5. Liberek, K., Marszalek, J., Ang, D., and Georgopoulos, C. (1991) *Proc. Natl. Acad. Sci. U.S.A. 88*, 2874−2878.
6. Banecki, B., and Zylicz, M. (1996) *J. Biol. Chem. 271*, 6137−6143.
7. Wall, D., Zylicz, M., and Georgoploulos, C. (1994) *J. Biol. Chem. 269*, 5446−5451.
8. Wall, D., Zylicz, M., and Georgopoulos, C. (1995) *J. Biol. Chem. 270*, 2139−2144.
9. Szabo, A., Korszun, R., Hartl, F. U., and Flanagan, J. (1996) *EMBO J. 15*, 408−417.
10. Jordan, R., and McMacken, R. (1995) *J. Biol. Chem. 270*, 4563−4569.
11. Auger, I., and Roudier, J. (1997) *J. Clin. Invest. 99*, 1818−1822.
12. Tsai, J., and Douglous, M. G. (1996) *J. Biol. Chem. 271*, 9347−9354.
13. Greene, M. K., Maskos, K., and Landry, S. J. (1998) *Proc. Natl. Acad. Sci. 95*, 6108−6113.
14. Huang, K., Flanagan, J. M., and Prestegard, J. H. (1999) *Protein Science 8*, 203−214.
15. Szyperski, T., Pellecchia, M., Wall, D., Georgopoulos, C., and Wüthrich, K. (1994) *Proc. Natl. Acad. Sci. U.S.A. 91*, 11343−11347.
16. Hill, R. B., Flanagan, J. M., and Prestegard, J. H. (1995) *Biochemistry 34*, 5587−5596.
17. Pellecchia, M., Szyperski, T., Wall, D., Georgopoulos, C., and Wüthrich, K. (1996) *J. Mol. Biol. 260*, 236−250.
18. Qian, Y. Q., Patel, D., Hartl, F. U., and McColl, D. J. (1996) *J. Mol. Biol. 260*, 224−235.
19. Clore, G. M., Driscoll, P. C., Wingfield, P. T., and Gronenborn, A. M. (1990) *Biochemistry 29*, 7387−7401.
20. Cheng, J.-W, Lepre, C. A., and Moore, J. M. (1994) *Biochemistry 33*, 4093−4100.
21. Zheng, Z., Czaplicki, J., and Jardetzky, O. (1995) *Biochemistry 34*, 5212−5223.
22. Habazettl, J., Myers, L. C., Yuan, F., Verdine, G. L., and Wagner, G. (1996) *Biochemistry 35*, 9335−9348.
23. Farrow, N. A., Zhang, O., Forman-Kay, J. D., and Kay, L. E. (1997) *Biochemistry 36*, 2390−2402.
24. Lipari, G., and Szabo, A. (1982) *J. Am. Chem. Soc. 104*, 4546−4559.
25. Lipari, G., and Szabo, A. (1982) *J. Am. Chem. Soc. 104*, 4559−4570.
26. Clore, G. M., Szabo, A., Bax, A., Kay, L. E., Driscoll, P. C., and Gronenborn, A. M. (1990) *J. Am. Chem. Soc. 112*, 4989−4991.
27. Deverell, C., Morgan, R. E., and Strange, J. H. (1970) *Mol. Phys. 18*, 553−559.
28. Akke, M., and Palmer, A G. III. (1996) *J. Am. Chem. Soc. 118*, 911−912.
29. Akke, M., Liu, J., Cavanagh, J., Erickson, H. P., and Palmer, A. G. III. (1998) *Nature Struct. Biol. 5*, 55−59.
30. Cordier, F., Brutscher, B., and Marion, D. (1996) *J. Biomol. NMR 7*, 163−168.
31. Dayie, K. T., and Wagner, G. (1997) *J. Am. Chem. Soc. 119*, 7797−7806.
32. Engleke, J., and Rüterjans, H. (1997) *J. Biolmol NMR 9*, 63−78.
33. Zeng, L., Fischer, M. W. F., and Zuiderweg, E. R. P. (1996) *J. Biolmol. NMR 7*, 157−162.
34. Fischer, M. W. F., Zeng. L., Pang, Y., Hu, W., Majumdar, A., and Zuiderweg, E. R. P. (1997) *J. Am. Chem. Soc. 119*, 12629−12642.
35. Farrow, N. A., Muhandiram, R., Singer, A. U., Pascal, S. M., Kay, C. N., Gish, G., Shoelson, S. E., Pawson, T., Forman-Kay, J. D., and Kay, L. E. (1994) *Biochemistry 33*, 5984−6003.

36. Sklenar, V., Torchia, D. A., and Bax, A. (1987) *J. Magn. Resn. 73*, 375−376.
37. Grzesiek, S., and Bax, A. (1992) *J. Magn. Resn. 99*, 201−207.
38. Marion, D., Ikura, M., Tschudin, R., and Bax, A. (1989) *J. Magn. Resn. 85*, 393−399.
39. Emsley, L., and Bodenhausen, G. (1990) *Chem. Phys. Lett. 165*, 469−476.
40. Boyd, J., Hommel, U., and Campbell, I. D. (1990) *Chem. Phys. Lett. 175*, 477−482.
41. Palmer, A. G. III, Skelton, N. J., Chazin, W. J., Wright, P. E., and Rance, M. (1992) *Mol. Phys. 75*, 699.
42. Davis, D. G., Perlman, M. E., and London, R. E. (1994) *J. Magn. Resn. 104 B*, 266−275.
43. Abragam, A. (1961) *The Principles of Nuclear Magnetism*, Clarendon Press, Oxford.
44. Hiyama, Y., Niu, C., Silverton, J. V., Bavoso, A., and Torchia, D. A. (1988) *J. Am. Chem. Soc. 110*, 2378.
45. Peng, J. W., Thanabal, V., and Wagner, G. (1991) *J. Magn. Resn. 94*, 82−100.
46. Woessner, D. E. (1962) *J. Chem. Phys. 37*, 647−654.
47. Orekhov, V. Yu., Nolde, D. E., Golovanov, A. P., Korzhnev, D. M., and Arseniev, A. S. (1995) *Appl. Magn. Reson. 9*, 581−588.
48. Garsia de la Torre, J., and Bloomfield, V. A. (1977) *Biopolymers 16*, 1747−1763.
49. Garsia de la Torre, J., and Bloomfield, V. A. (1977) *Biopolymers 16*, 1765−1778.
50. Garsia de la Torre, J., and Bloomfield, V. A. (1981) *Q. Rev. Biophys. 14*, 81−139.
51. Pastor, R. W., and Karplus, M. (1988) *J. Phys. Chem. 92*, 2636−2641.
52. Lee, B., and Richards, F. M. (1971) *J. Mol. Biol. 55*, 379−400.
53. Bevington, P. R., and Robinson, D. K. (1992) *Data Reduction and Error Analysis for the Physical Science*, 2nd ed., pp 205−209, McGraw-Hill, Inc. New York.
54. Venable, R. M., and Pastor, R. W. (1988) *Biopolymers 27*, 1001−1014.
55. Tjandra, N., Feller, S. E., Pastor, R. W., and Bax, A. (1995) *J. Am. Chem. Soc. 117*, 12562−12566.
56. Koradi, R., Billeter, M., Wuthrich, K. (1996) *J. Mol. Graphics 14*, 51−55.
57. Gassler, C. S., Buchberger, A., Laufen, T., Mayer, M. P., Schroder, H., Valencia, A., and Bukau, B. (1998) *Proc. Natl. Acad. Sci. 95*, 15229−15234.
58. Suh, W. C., Burkholder, W. F., Lu, C. Z., Zhao, X., Gottesman, M. E., Gross, C. A. (1998) *Proc. Natl. Acad. Sci. 95*, 15223−15228.
59. Klostermeier, D., Seidel, R., Reinstein, J. (1999) *J. Mol. Biol. 287*, 511−525.
60. Russell, R., Karxai, A. W., Mehl, A. F., McMacken, R. (1999) *Biochemistry 38*, 4165−4176.

BI990263+